aerospace

MDPI

Article

Retrieval of the Stratospheric Density by the Star Occultation

Kedong Wang [1,*], Zhennan Li [1] and Shaoxiong Zhang [2]

[1] School of Astronautics, Beihang University, Beijing 100191, China
[2] Institute of Remote Sensing Satellite, China Academy of Space Technology, Beijing 100094, China
* Correspondence: wangkd@buaa.edu.cn; Tel.: +86-136-9157-2701

Abstract: The navigation by the stellar refraction is important for a LEO (Low-Earth-Orbit) satellite, especially in a GNSS (Global Navigation Satellite System)-denied environment, since it is totally autonomous. However, the biggest barrier to the accurate navigation by the stellar refraction lies in the accurate stratospheric density. Therefore, the retrieval of the stratospheric density by the star occultation is proposed in this paper to acquire the stratospheric density globally with the high accuracy. Compared with the retrieval of the stratospheric density by the GPS (Global Positioning System) radio occultation, the retrieval by the star occultation can achieve a high vertical resolution. The retrieval of the stratospheric density by the star occultation is first derived in principle. Then, the performance of the retrieval, including the spatial resolution, the atmospheric attenuation, and the accuracy, was investigated in detail. The performance of the retrieval was also comprehensively verified by simulations. The simulation results prove that the retrieval of the stratospheric density by the star occultation can achieve a similar accuracy to that by the GPS radio occultation, but it has a higher vertical resolution than that by the GPS radio occultation, which is good for improving the accuracy of the navigation by the stellar refraction.

Keywords: autonomous navigation; stellar refraction; remote sensing; GPS; occultation

check for updates

Citation: Wang, K.; Li, Z.; Zhang, S. Retrieval of the Stratospheric Density by the Star Occultation. *Aerospace* **2023**, *10*, 313. https://doi.org/10.3390/aerospace10030313

Academic Editor: M. Reza Emami

Received: 25 August 2022
Revised: 9 March 2023
Accepted: 17 March 2023
Published: 22 March 2023

1. Introduction

Unlike GNSS (Global Navigation Satellite System), the navigation by the stellar refraction for a spacecraft is totally autonomous [1,2]. Compared with the navigation by the angular separation between a star and the Earth, for the other popular autonomous solution, only having the 1km-level positioning, the stellar refraction can achieve 100 m-level positioning [3]. Hence, the navigation by the stellar refraction is crucial for a spacecraft, especially the LEO (Low-Earth-Orbit) satellite, to position autonomously and accurately.

The navigation by the stellar refraction was initially proposed for the Apollo spacecraft, although it was not implemented at that time [4]. Later, the researchers from CSDL (Charles Stark Draper Laboratory) demonstrated that the navigation by the stellar refraction can achieve the 100 m-level positioning by fusing the tangent height derived from the refraction data with the spacecraft orbit data in a Kalman filter by simulations [3]. It should be noted that the atmospheric density error was assumed to be no greater than 1.1% in the simulations, while the variation of the atmospheric density may be as large as or even greater than 10% in the stratosphere [5,6]. In order to reduce the impact of the atmospheric density variation on the stellar refraction, the altitude range of interest is usually limited from 20 km to 50 km [7]. However, the inaccurate stratospheric density is still the biggest barrier to improve the navigation accuracy by the stellar refraction, which will be addressed in this paper.

The atmospheric density can be obtained by the direct method or the remote sensing. The direct method includes the drag-derived measurement by the LEO spacecraft [8] and the measurement by the meteorological rocket and balloon [9]. The atmospheric drag has been widely employed to derive the upper thermospheric density, but it cannot measure the stratospheric density [8]. Although both the meteorological rocket and balloon can

measure the stratospheric density accurately, it is very difficult for them to measure the density globally with a high resolution [10]. The remote sensing includes the ground-based and the space-based. The ground-based remote sensing can be divided into the passive and the active. Compared with the passive remote sensing, the active remote sensing by LiDAR (Light Detection and Ranging) or Radar (Radio Detection and Ranging) can retrieve the atmospheric density at high spatial and temporal resolutions locally, but it is still difficult for it to obtain the density globally [11,12]. However, it is convenient for the space-based remote sensing, such as the GPS (Global Positioning System) radio occultation, to retrieve the atmospheric density globally [13]. Therefore, the GPS radio occultation has been widely employed to obtain the atmospheric density profile from ground to the ionosphere at the high spatial and temporal resolutions globally [14,15]. The atmospheric density error retrieved by the GPS radio occultation is even less than 0.3% below 30 km, but the vertical resolution of the retrieval is limited by the diffraction, i.e., the diameter of the first Fresnel zone [16]. At the GPS L1 wavelength of 19 cm, the vertical resolution of the retrieval is about 1.4km if the receiver is mounted on a LEO spacecraft, such as a 700 km altitude orbit satellite [16]. Therefore, many efforts have been devoted to improve the vertical resolution of the retrieval by the GPS radio occultation [17,18].

In fact, the diameter of the first Fresnel zone is related to the wavelength [16]. If the wavelength is reduced, the diffraction-limited vertical resolution of the retrieval will be improved accordingly. For example, if the wavelength is as short as 550 nm, the diffraction-limited vertical resolution will be as high as 2.5 m so that the diffraction will not be the limit to the vertical resolution of the retrieval anymore. The star occultation was employed to retrieve trace gas, such as aerosol and ozone, in the stratosphere [19,20]. However, the star occultation has not been used to retrieve the stratospheric density up to now. Hence, this paper will investigate the retrieval of the stratospheric density by the star occultation for the first time, which is the main contribution in this paper. The refracted rays of the starlight in the visible band will be sensed by a star sensor mounted on a LEO satellite. The star occultation is similar to the GPS radio occultation in principle, but the starlight's wavelength is far shorter than the GPS signals. It should be noted that the retrieval of the atmospheric density by the star occultation is only applicable to the altitude range of 20–50 km, the interested range of the navigation by the stellar refraction.

The rest of the paper is organized as follows. The principle of the retrieval of the stratospheric density by the star occultation was provided first. The performance of the retrieval, including the spatial resolution and the atmospheric attenuation, was analyzed further. The retrieval accuracy was also studied. Simulations demonstrate the feasibility of the retrieval to some extent. Finally, the concluding remarks are summarized.

2. Retrieval of the Stratospheric Density by the Star Occultation

As illustrated in Figure 1, when the rays of starlight pass through the atmosphere, they will be refracted. Take the ray, the lower second one illustrated in Figure 1, as an example to describe its refraction. Before it enters the atmosphere, it passes along the direct path whose unit vector is $\mathbf{u}$, which will be called the direct starlight hereinafter. After it enters the atmosphere from the point p_i, it will be refracted by the atmosphere. It will bend down to the Earth before it passes through the tangent point p_g, the closest point to the Earth. The radius vector at the tangent point is $\mathbf{r}_g$ with the norm r_g, i.e., $r_e + h_g$, where r_e and h_g are the Earth radius and the tangent height, respectively. The ray will bend up to the sky after it passes through the tangent point. It will pass out the atmosphere at the point p_o. There is no impact of the atmosphere on the ray after the point p_o. The radius vector $\mathbf{r}$ is the direction from the Earth center to a point at the refracted path of the ray. The refraction angle, α, observed from the satellite, is the angle between the tangent at the point p_i, i.e., the vector $\mathbf{u}$, and that at the point p_o, i.e., the apparent path. The satellite has the radius vector $\mathbf{r}_s$ and the zenith angle θ_s. The vector $\mathbf{r}_a$ is the direction from the Earth center to its foot of a perpendicular at the apparent path. The norm of $\mathbf{r}_a$ is $r_a = r_e + h_a$, where h_a is the apparent height viewed from the satellite.

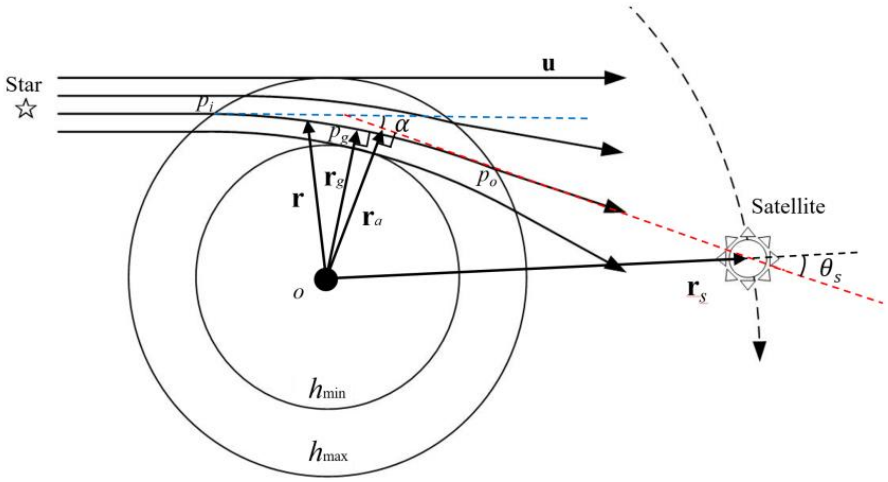

Figure 1. Schematic diagram of the star occultation.

The star occultation is the process of viewing the rays from the direct to the obstructed by the Earth. For one thing, the denser the atmosphere is, the larger the refraction angle is. Therefore, the refraction angle is large when the starlight is close to the ground, and vice versa. Although the large refraction angle is good for improving its observing accuracy, the lowest tangent height is usually set as 20 km for the stellar refraction since the atmospheric density close to the troposphere fluctuates significantly [21]. The scintillation over 20 km due to internal gravity waves, turbulence, and other irregularities may impact on the stellar refraction to some extent, but its impact can be eased significantly by increasing the exposure time [6]. The impact of scintillation will not be considered in this paper anymore. For another, the refraction angle is small when the starlight is far from the ground. If the refraction angle is too small to be sensed by the star sensor, the corresponding height will be the upper limit of the occultation in fact. Therefore, the star occultation refers to the process of viewing the refracted starlight in a range of the tangent height, [hmin, hmax], as illustrated in Figure 1.

In Figure 1, when a ray of the refracted starlight is viewed by a star sensor mounted on a LEO satellite, the refraction angle, α, can be derived as [22],

$$\alpha = 2n_g r_g \int_1^{n_g} \frac{\mathrm{d}n}{n\sqrt{n^2r^2 - n_g^2 r_g^2}} \tag{1}$$

where n is the index of refraction, r is the norm of the radius vector $\mathbf{r}$, and the subscript 'g' refers to the tangent point. In (1), the spherically stratified atmosphere is assumed. Using an Abelian transformation, (1) can be inverted as [23],

$$\ln n = \frac{1}{\pi}\int_a^{\infty} \frac{\alpha}{\sqrt{x^2 - a^2}}\mathrm{d}x \tag{2}$$

where $x = nr$ and $a = n_g r_g$. Since the atmosphere is assumed as the spherically stratified media, the ray obeys Snell's law as [22],

$$nr\sin\theta = \text{constant} \tag{3}$$

where θ is the zenith angle of the ray measured from the radius vector. At the tangent point, θ is 90°. Since the measurement is carried out from the LEO satellite at $r = r_s$, $n_s \approx 1$, and the known θ_s, (3) can be rewritten as,

$$nr = r_s \sin\theta_s = r_e + h_a \tag{4}$$

where r_s is the norm of $\mathbf{r}_s$ and n_s is the refractive index at the satellite position. Substitute (4) into (2) and yield,

$$\ln n = \frac{1}{\pi}\int_{h_{a\min}}^{h_\infty} \frac{\alpha}{\sqrt{(h_a + r_e)^2 - (h_{a\min} + r_e)^2}} \mathrm{d}h_a \tag{5}$$

where $h_{a\min}$ is the minimum apparent height of the ray and h_∞ is the apparent height of the direct starlight. If the values of α in the range of $[h_{a\min}, h_\infty]$ are measured by the star sensor, the values of n can be retrieved by (5). Since there is a maximum height $h_{\max}$ in the occultation as mentioned above, h_∞ should be revised as $h_{a\max}$, the apparent height at the tangent height of $h_{\max}$.

There is the Gladstone and Dale's law as,

$$n = 1 + k_{G-D}\rho \tag{6}$$

where k_{G-D} is the Gladstone–Dale coefficient related to the starlight wavelength λ and ρ is the atmospheric density [24]. According to (6), ρ can be derived from n linearly. That is, the atmospheric density can be retrieved by the measured refraction angle.

In the implementation, the refraction angles will be sampled discretely so that (5) should be discretized. Given that $N+1$ samples of the refraction angle and the apparent height, i.e., $(\alpha_l, h_{a,l})(l = 1, 2, \cdots, N+1)$, are obtained in the occultation. Let $\eta = h_a + r_e$. Assume that the refraction angle α is proportional to η approximately in a sampling interval as,

$$\beta_l = \frac{\alpha_{l+1} - \alpha_l}{\eta_{l+1} - \eta_l}, l = 1, \cdots, N \tag{7}$$

Substitute (7) into (5) and yield,

$$\begin{aligned} \ln n_l \quad = & \frac{1}{\pi}\sum_{j=l}^{N}\Bigg\{\beta_j\eta_l\left(\sqrt{\left(\frac{\eta_{j+1}}{\eta_l}\right)^2 - 1} - \sqrt{\left(\frac{\eta_j}{\eta_l}\right)^2 - 1}\right) \\ & + (\alpha_j - \beta_j\eta_j)\ln\left(\sqrt{1 + \left(\frac{\eta_{j+1}}{\eta_l}\right)^2} + \frac{\eta_{j+1}}{\eta_l}\right) \\ & - (\alpha_j - \beta_j\eta_j)\ln\left[\sqrt{1 + \left(\frac{\eta_j}{\eta_l}\right)^2} + \frac{\eta_j}{\eta_l}\right]\Bigg\} \end{aligned} \tag{8}$$

By substituting n_l into (6), the atmospheric density can be derived. Obviously, there is the discretization error in (8). The smaller the sampling interval is, the less the discretization error is. In the following, the retrieval performance by measuring the refraction angle will be addressed in detail.

3. Spatial Resolution

Both the vertical and the horizontal resolutions are studied herein. The former is related to the duration of the occultation and the sampling frequency of the refraction angle. The latter is mainly determined by the number of the satellites, the orbital elements of the satellites, and the magnitude threshold of the star sensor. In this paper, only one satellite is assumed for the retrieval of the stratospheric density by the star occultation.

3.1. Vertical Resolution

Unlike the GPS radio occultation, the diffraction has little impact on the vertical resolution of the retrieval of the stratospheric density by the star occultation. The diameter of the first Fresnel's zone D_F, one of the limits on the vertical resolution, is given by [16],

$$D_F = 2\sqrt{\lambda\frac{L_T L_R}{L_T + L_R}} \tag{9}$$

where L_T and L_R are the distances from the star and the star sensor to the atmospheric limb, respectively. Usually, $L_T \gg L_R$ so that (9) can be rewritten approximately as,

$$D_F \approx 2\sqrt{\lambda L_R} \tag{10}$$

L_R is about 3100 km for a star sensor in a 700 km altitude orbit. At the starlight wavelength of 550 nm, the diameter is about 2.5 m while it is as large as 1.4 km at the GPS L1 wavelength of 19 cm. Therefore, the limit of the diffraction on the vertical resolution is negligible for the retrieval of the stratospheric density in the visible region of (400 nm, 760 nm).

However, the vertical resolution of the retrieval of the stratospheric density is mainly dominated by the duration of the occultation and the sampling frequency of the refraction angle. Since the range of the altitude is constant in the occultation, the vertical resolution will be higher if the duration of the occultation lasts longer. The duration of the occultation is related to the orbit. Figure 2 depicts the duration of the occultation with the satellite orbits. In Figure 2, the duration of the occultation decreases with the increase of the orbit. If only the vertical resolution is concerned, the satellite's orbit should be as low as possible. Of course, the atmospheric drag will increase significantly with the decrease of the orbit. Hence, the orbit of the satellite should be determined by trading off the vertical resolution against the satellite's running life. Moreover, the vertical resolution is also related to the sampling frequency of the refraction angle, or the output frequency of the star sensor equivalently. The higher the output frequency of the star sensor is, the higher the vertical resolution is. It should be noted that the output frequency depends on the exposure time of the star sensor. Figure 3 depicts the vertical resolution with the orbit when the output frequency of the star sensor is 10 Hz. In Figure 3, the vertical resolution is as high as 180 m when the orbit is 200 km. Even though the orbit is as high as 2000 km, the vertical resolution is still less than 450 m, which is far higher than the vertical resolution by the GPS radio occultation.

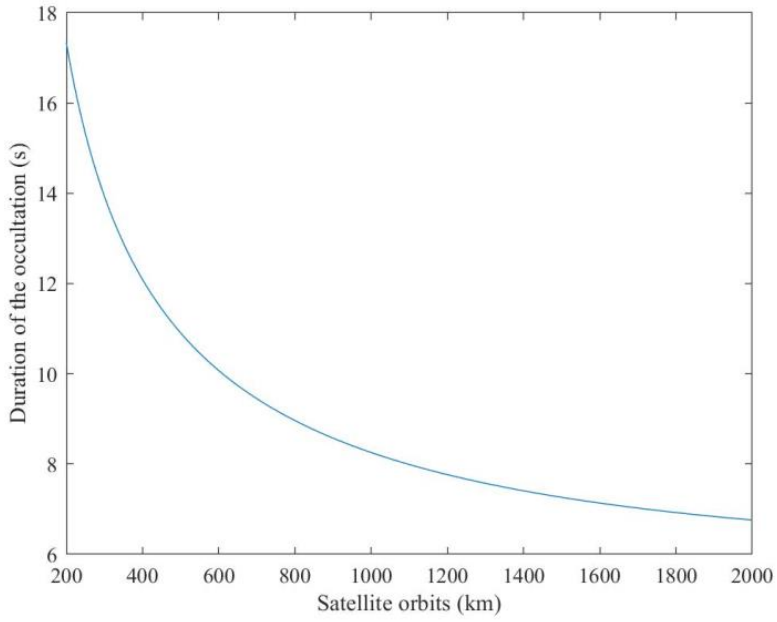

Figure 2. Duration of the occultation with the satellite orbits.

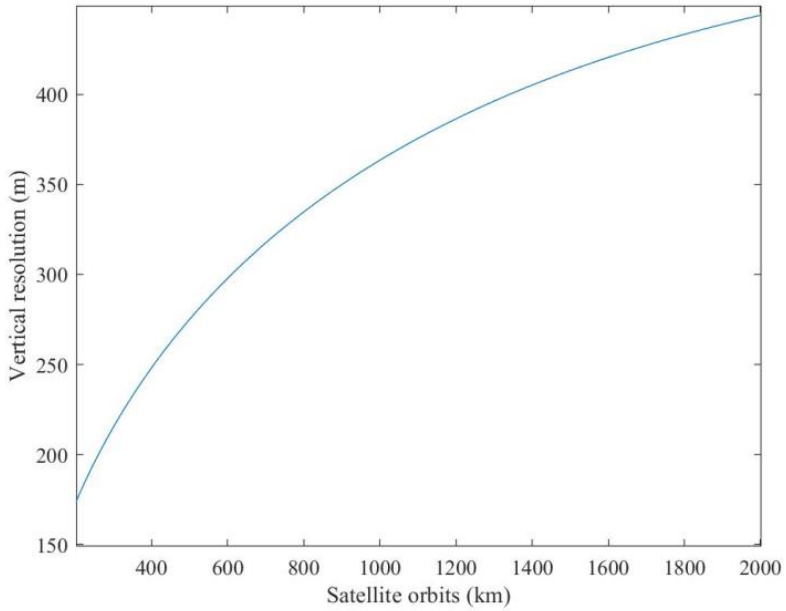

Figure 3. Vertical resolution with the satellite orbits.

3.2. Horizontal Resolution

Due to the rotation of the Earth, the longitude interval of the retrieval of the stratospheric density ΔL can be calculated as,

$$\Delta L = 360\omega_e \sqrt{\frac{r_s^3}{GM}} \tag{11}$$

where ω_e is the rotation rate of the Earth and GM is the geocentric gravitational constant. Hence, the low orbit is good for reducing the longitude interval of the retrieval.

However, the coverage of the retrieval of the stratospheric density in the latitude range is related to not only the orbit (its inclination i and Right Ascension of the Ascending Node (RAAN) Ω) but also the star sensor (its direction of the optical axis and the magnitude threshold). Figure 4 illustrates the relationship of the latitude range of the retrieval with the inclination i and the angle between the optical axis of the star sensor and the orbital plane ψ. In Figure 4a, the optical axis of the star sensor does not lie in the orbital plane and $i < 90^\circ$. The two cases of the occultation at the minimum and the maximum latitudes are illustrated. The green area shows the latitude range of the retrieval. Obviously, when the optical axis of the star sensor lies in the orbital plane ($\psi = 0^\circ$), the polar orbit ($i = 90^\circ$) should be employed to accomplish the retrieval in the whole latitude range, as illustrated in Figure 4b. Figure 5 depicts the latitude range of the retrieval with the RAAN Ω and the magnitude threshold when $\psi = 0^\circ$, $i = 90^\circ$, and the magnitude thresholds of the viewed stars are 5.5 Mv, 6.0 Mv, and 6.5 Mv, respectively. Mv refers to the apparent magnitude. If the latitude range approaches to 100%, the stratospheric density in all the latitude range of [−90 deg, 90 deg] can be retrieved approximately. In Figure 5, the latitude range of the retrieval is large when Ω is close to 90°. Moreover, the impact of Ω on the latitude range of the retrieval decreases with the increase of the magnitude thresholds, since more dark stars can be observed if the magnitude threshold of the viewed stars is improved.

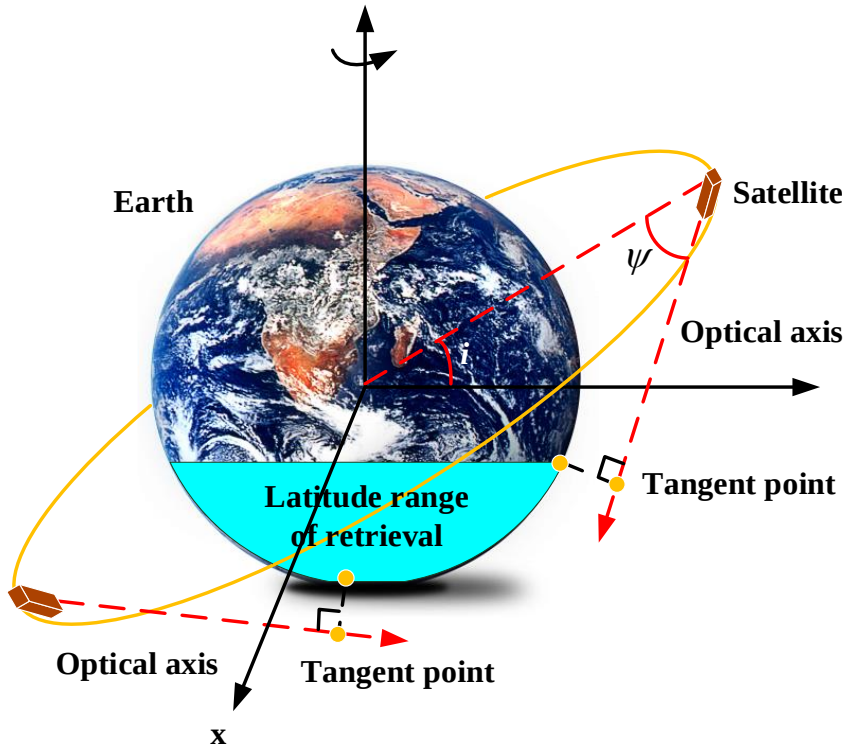

(**a**)

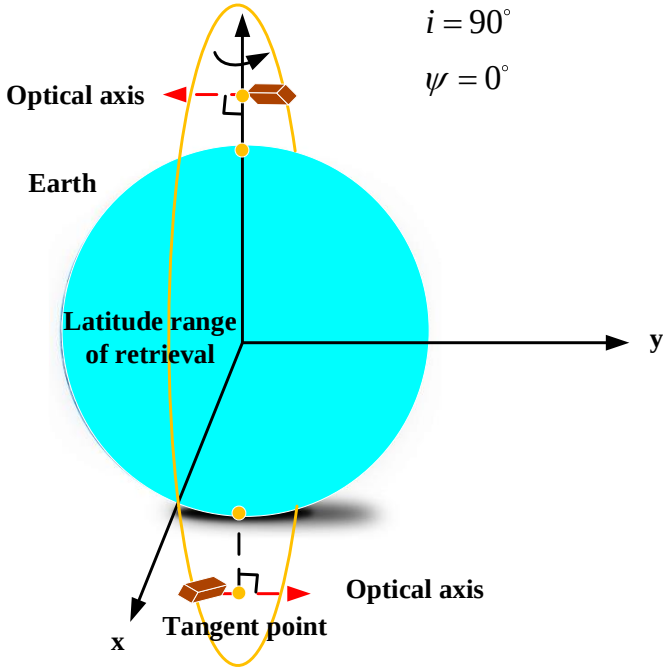

(**b**)

Figure 4. Schematic diagram of the latitude range of the retrieval. (**a**) Optical axis does not lie in the orbital plane and $i < 90°$. (**b**) Optical axis lies in the orbital plane and $i = 90°$.

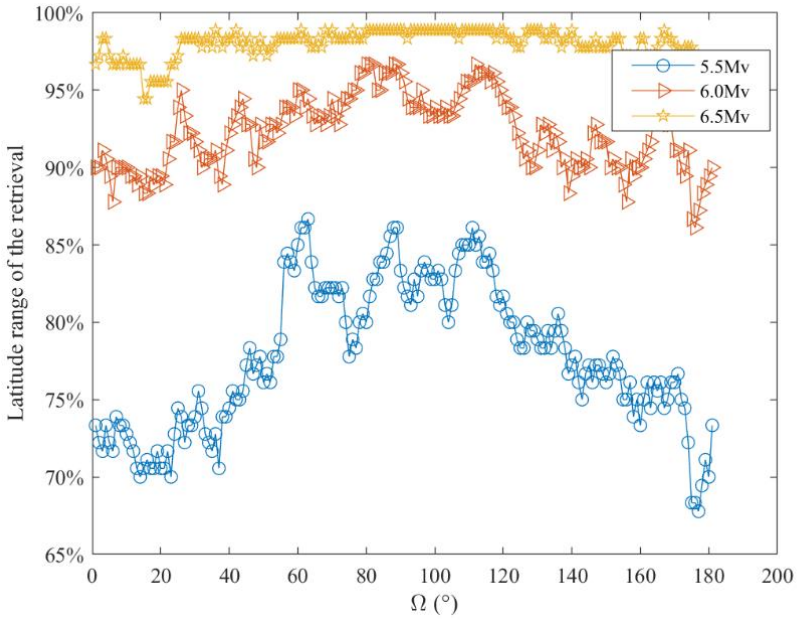

Figure 5. Latitude range of the retrieval with RAAN.

4. Atmospheric Attenuation

When the ray of the starlight pass through the atmosphere, it is not only refracted but also attenuated. The atmospheric attenuation is related to the wavelength. Since the starlight energy is contributed mainly by the visible spectral region, only the visible spectrum is analyzed herein. In this section, the wavelengths of 450 nm, 550 nm, and 650 nm will be taken as the typical examples to analyze the attenuation. As analyzed in [14], the refractive dispersion, the molecular scattering, and the ozone absorption provide the primary loss for the visible light passing through the stratosphere, which will be addressed in detail in the following. The other minor attenuations, such as Mie scattering, will not be discussed anymore [22].

4.1. Refractive Dispersion

The reduction of the intensity of the transmitted radiation due to refraction can be approximated as [24],

$$k_{dr} = \frac{1}{1 + \frac{r_s \cos\varphi}{H}\sqrt{\frac{2\pi r_g}{H}}k\rho_g} \tag{12}$$

where k_{dr} is the ratio of the intensity after being attenuated to that before being attenuated, φ is the angle between the direct starlight $\mathbf{u}$ and the radius vector $\mathbf{r}_s$, and H is the scale height. Figure 6 depicts the ratio with the tangent height. In Figure 6, the reduction of the intensity increases as the tangent height decreases. That is, although reducing the tangent height can observe the large refraction angle, not only will the retrieval accuracy be impacted by the variation of the atmospheric density close to ground significantly as mentioned above, but the intensity of the refracted starlight observed by the star sensor will be attenuated tremendously. Moreover, the variation with the wavelength is negligible.

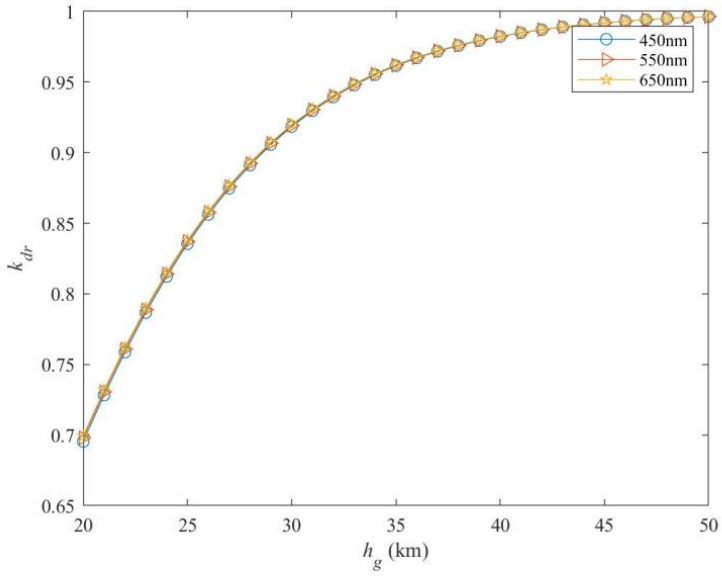

Figure 6. k_{dr} with the tangent height.

4.2. Molecular Scattering

The attenuation of the starlight with the wavelength of λ in the spherically stratified atmosphere due to the molecular scattering, k_{ms}, can be approximated as [24],

$$k_{ms} = \exp\left[-\frac{32\pi^4}{3\lambda^4}k^2 m\rho(2r_g + H)\sqrt{\frac{H}{2\pi r_g}}\right] \tag{13}$$

where k_{ms} is the ratio of the intensity of the starlight after being attenuated to that before being attenuated and m is the mass of a hypothetical air molecule. Figure 7 depicts the attenuation due to the molecular scattering with the tangent height. In Figure 7, the attenuation increases as the tangent height decreases, which is similar to that due to refractive dispersion. However, at the same tangent height, the starlight with a shorter wavelength will be attenuated more heavily than that with a longer wavelength.

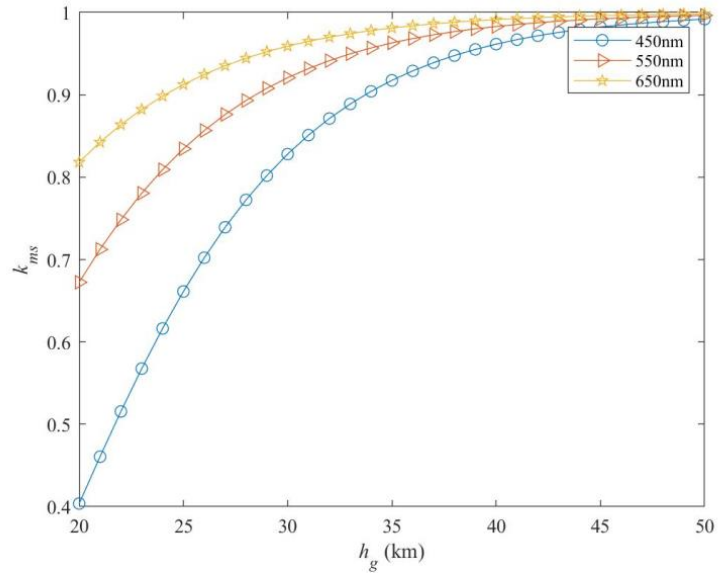

Figure 7. k_{ms} with the tangent height.

4.3. Ozone Absorption

Since the distribution of ozone with height varies with time, the standard ozone profile with altitude was employed herein to evaluate the impact of the ozone absorption on the starlight [23]. The attenuation of the starlight with the wavelength of λ in the spherically stratified atmosphere due to the ozone absorption, k_{oa}, can be approximated as [24],

$$k_{oa} = \exp\left(-k_{O_3} H_{O_3}\right) \tag{14}$$

where k_{O_3} is the coefficient of the ozone absorption and H_{O_3} is the equivalent ozone thickness in the starlight path. The coefficient k_{O_3} is related to the wavelength λ. In the standard ozone profile, the values of k_{O_3} with the wavelengths of 450 nm, 550 nm, and 650 nm are 0.007, 0.113, and 0.073, respectively [24]. Figure 8 depicts the attenuation due to the ozone absorption with the tangent height. In Figure 8, the attenuation due to the ozone absorption increases as the tangent height decreases too. It is also noted that the rays of the starlight with the wavelength of 550 nm are attenuated more significantly than that with the wavelength of 650 nm at the same tangent height. The rays of the starlight with a wavelength of 450 nm were attenuated slightly by the ozone absorption [24].

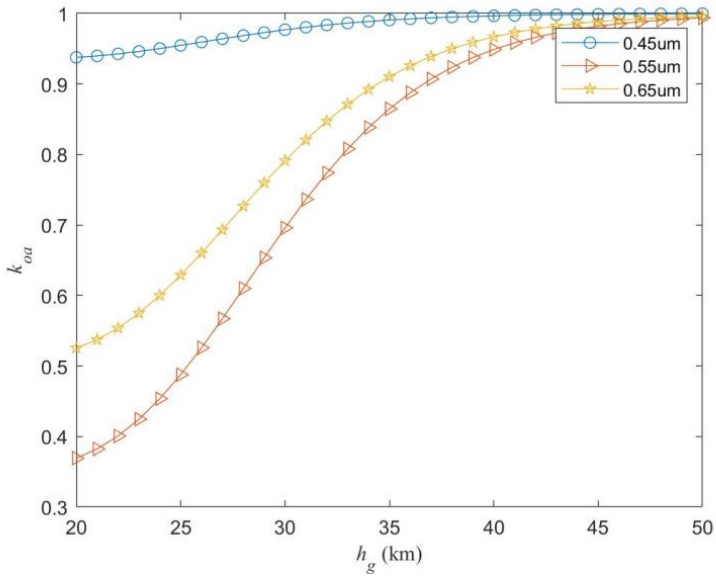

Figure 8. k_{oa} with the tangent height.

4.4. Impact on the Apparent Magnitude

Since the ray of the starlight passing through the stratosphere is mainly attenuated by the refractive dispersion, the molecular scattering, and the ozone absorption, the difference of the equivalent apparent magnitude between before and after being attenuated, $dMva$, can be calculated as [24],

$$dMva = -1.086 \ln(k_{dr} k_{ms} k_{oa}) \tag{15}$$

Figure 9 depicts the difference with the tangent height. As expected, the difference decreases as the tangent height increases. That is, the equivalent apparent magnitude is larger if the tangent height is lower. For example, if the ray of the starlight with the apparent magnitude of 5 Mv passes through the stratosphere at the tangent height of 20 km, its apparent magnitude will turn to 6.5 Mv when it is sensed by the star sensor according to (15). Hence, many stars will not be sensed by the star sensor in the occultation due to the attenuations, which is not good for improving the horizontal resolution of the retrieval of the density. Figure 10 depicts the horizontal coverage percentage with time if the latitude and longitude resolutions are 1° and 5°, respectively, and the magnitude threshold of the star sensor is 7 Mv. Since the Earth is rotating, the horizontal coverage percentage should increase with time. In Figure 10, the horizontal coverage percentage

decreases as the tangent height decreases. If the tangent height is 35 km, the horizontal coverage percentage approaches to 100% after 100 h. However, the horizontal coverage percentage is just about 82% after 160 h if the tangent height is 20 km. Hence, the tangent height should be as high as possible if only the attenuation is concerned. Otherwise, more satellites are required to improve the horizontal coverage.

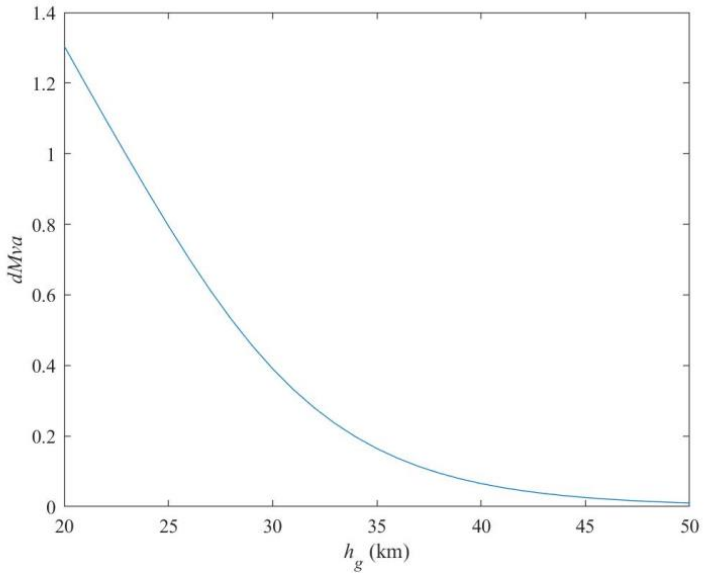

Figure 9. Difference of the equivalent apparent magnitude with the tangent height.

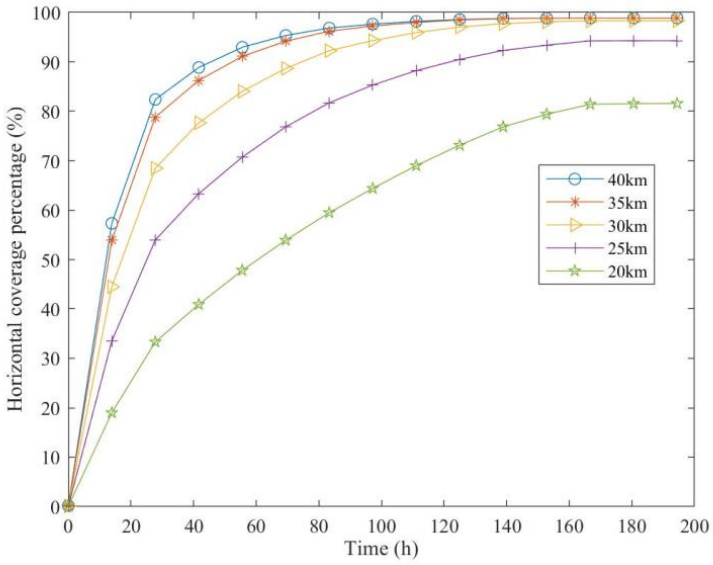

Figure 10. Horizontal coverage percentage with time.

5. Retrieval Accuracy

Before presenting the retrieved stratospheric density by the star occultation, the accuracy of the retrieval will be analyzed in this section by simulation. The accuracy of the retrieval is related to the refraction angle error, the assumption in the derivation, and the satellite position error mainly, which will be investigated in the following, respectively.

In the analysis, the orbit listed in Table 1 and the star sensor listed in Table 2 were employed.

Table 1. Orbital elements of the satellite.

Inclination	RAAN	Altitude	Eccentricity	Number of Satellites
90°	90°	300 km	0	1

Table 2. Specifications of the star sensor.

Output Frequency	FOV	Focal Plane	Magnitude Threshold
10 Hz	10° × 10°	1024 × 1024	7 Mv

5.1. Assumption-Derived Error

The retrieval of the stratospheric density by the star occultation was derived with some assumptions. Inevitably, the assumptions, including the spherically stratified atmosphere, the occultation starting from the highest tangent height $h_{\max}$, and the occultation implemented discretely, will lead to the error of the retrieval. Figure 11 depicts the relative error of the retrieval of the stratospheric density due to the assumptions with the tangent height by comparing with the real stratospheric density. The stratospheric density was retrieved by the method proposed in Section 2. The real stratospheric density was acquired from the NRLMSISE-00 data with the high resolution, which is introduced in Section 6. The NRLMSISE-00 data recommended by the International Committee on Space Research (COSPAR) was developed by the US Naval Research Laboratory [25]. It is based on both mass spectrometry and incoherent radar scatter data and drag and accelerometer data. In Figure 11, the assumption-derived error increases as the tangent height increases. The assumption-derived error is negligible when the tangent height is 20 km, but it is about 2.5% when the tangent height is 50 km. If the tangent height is no higher than 35 km, the assumption-derived error is no more than 0.5%.

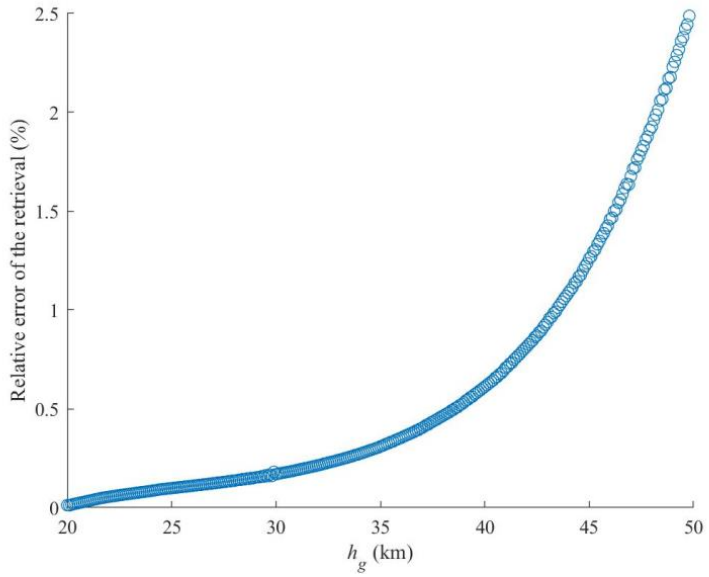

Figure 11. Relative error of the retrieval due to the assumptions with the tangent height.

5.2. Satellite Position Error

In (8), the retrieval of the index of the refraction uses a series of the apparent heights in the occultation. According to the geometry of the refraction, the apparent height can be calculated as [26],

$$h_a = \sqrt{|\mathbf{r}_s|^2 - |\mathbf{r}_s \cdot \mathbf{u}|^2} + |\mathbf{r}_s \cdot \mathbf{u}| \tan \alpha - r_e - b \tag{16}$$

where b is a small value that can be neglected. In (16), the error of the apparent height is mainly contributed by the uncertainty of the satellite position and the refraction angle error, which will lead to the error of the retrieval.

Fortunately, the LEO satellite can achieve 10 m-level positioning with a GNSS receiver. Figure 12 depicts the relative error of the retrieval of the stratospheric density due to the satellite position error with the tangent height by 600 times of the Monte Carlo simulations. In Figure 12, the relative error of the retrieval due to the satellite position error is irrelative with the tangent height. The RMS (Root Mean Squared) values of the relative error of the retrieval are 0.039%, 0.055%, and 0.061%, respectively, when the satellite position errors are 10 m, 50 m, and 100 m, respectively. Hence, the satellite position error has little impact on the accuracy of the retrieval.

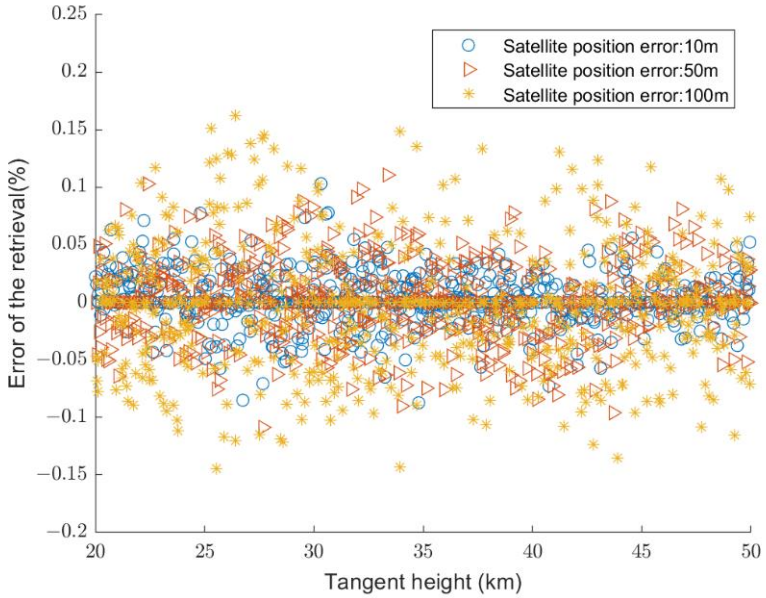

Figure 12. Relative error of the retrieval due to the satellite position error with the tangent height.

The impact of the refraction angle error on the apparent height, or the retrieval, will be addressed in the following.

5.3. Refraction Angle Error

Since the refraction angle is the only measurement used in the retrieval of the stratospheric density by the star occultation, its error will impact on the accuracy of the retrieval directly. Figure 13 depicts the RMS values of the relative error of the retrieval of the stratospheric density due to the refraction angle error with the tangent height by 600 times of the Monte Carlo simulations. In Figure 13, at the same tangent height, the relative error of the retrieval increases as the refraction angle error increases. Moreover, the relative error of the retrieval increases as the tangent height increases either. The main reason is that if the tangent height is higher, the refraction angle will be smaller, while its relative error will be larger. Compared with Figures 11 and 12, the refraction angle error impacts more significantly on the accuracy of the retrieval than the assumption-derived error and the satellite position error. Therefore, the accuracy of the refraction angle should be improved if possible.

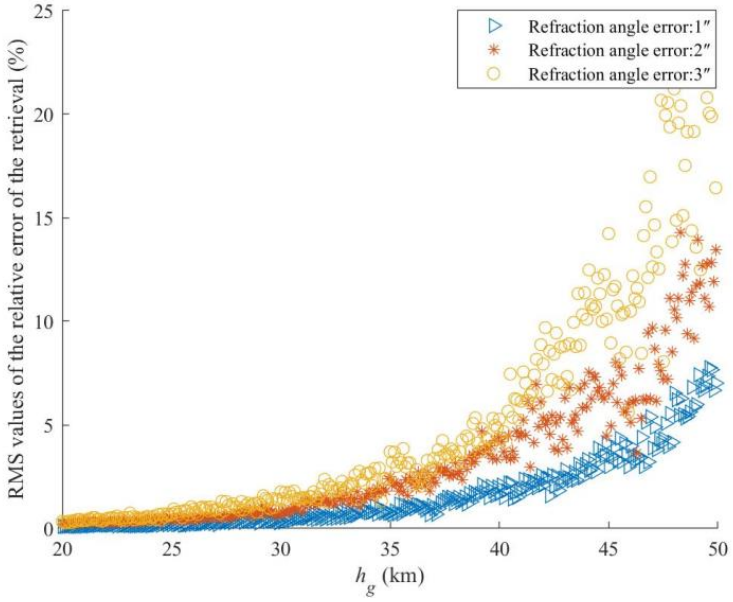

Figure 13. Relative error of the retrieval due to the refraction angle error with the tangent height.

6. Simulations

Herein, the accuracy of the retrieval of the stratospheric density by the occultation will be verified by simulations comprehensively. The orbit listed in Table 1 and the star sensor listed in Table 2 are still employed in the following simulations. The flowchart of the simulations is illustrated in Figure 14.

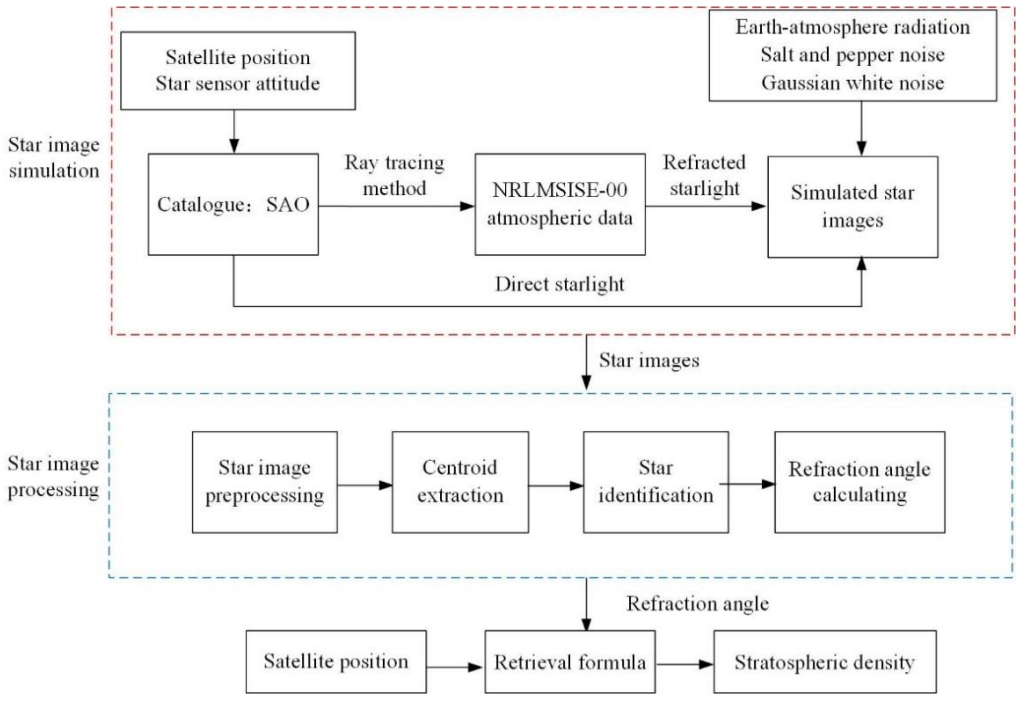

Figure 14. The flowchart of the simulations.

The NRLMSISE-00 data, whose resolutions in the latitude, the longitude, and the altitude directions were set as 0.5°, 0.5°, and 10 m, respectively, are treated as the reference, i.e., the real atmospheric data.

The star images are simulated using the SAO (Smithsonian Astrophysical Observatory) star catalogue J2000. As listed in Table 2, only the stars with the magnitude no greater than 7 Mv were simulated. The rays of the refracted starlight are simulated by the ray tracing method. The attenuation due to the refractive dispersion, the molecular scattering, and the ozone absorption were considered in simulating the refracted stars. Except for the Gaussian white noise and the salt-and-pepper noise, the earth–atmosphere radiation was also simulated in the star images. Figure 15 depicts a simulated star image output by the star sensor. The white points in the image are the viewed stars. In the upper part of the image, the background is black since there is no impact of the atmosphere. The starlights in the upper part are not refracted, but those in the lower part are refracted and attenuated by the atmosphere. Since the lowest part of the image is close to the ground, some starlights are blocked. The refracted starlights are attenuated by the atmosphere either. The simulated atmospheric radiation from the Earth to space in the visible band of the star sensor makes the lower part of the image white. There is both Gaussian white noise and salt-and-pepper noise in the image.

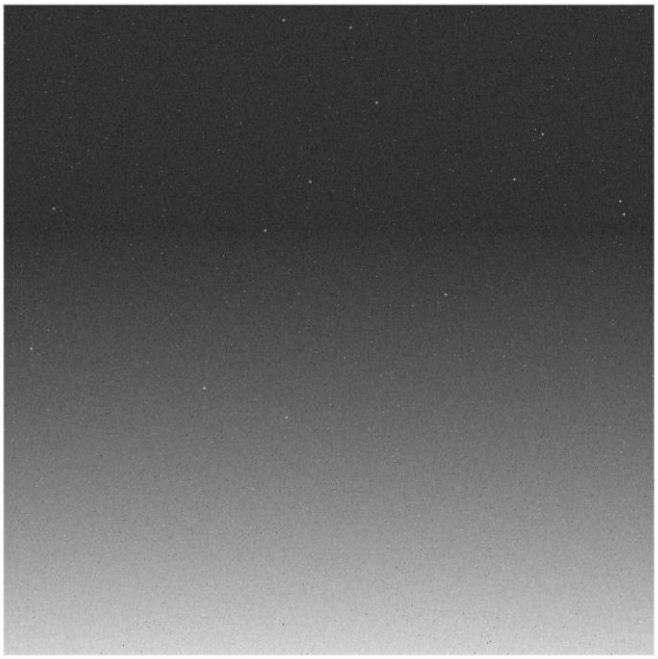

Figure 15. Simulated star image output by the star sensor.

The simulated images were processed to acquire the refraction angle. Both the refraction angle and the satellite position were used to retrieve the stratospheric density. Figure 16 depicts the relative error of the retrieved density with the tangent height by the Monte Carlo simulation. In total, 10,000 simulations were run to acquire the 10,000 relative error curves in Figure 16. The RMS values were also plotted in Figure 16. Figures 17 and 18 depict the retrieved density with the tangent height and its relative error in one simulation, respectively. In Figure 16, the relative error of the retrieval increases as the tangent height increases. The RMS value of the error of the retrieval is 0.9% at the tangent height of 30 km, while it is about 4.5% at the tangent height of 40 km. In Figures 17 and 18, the relative error of the retrieval also increases with the increase of the tangent height, which coincides with the result in Figure 16.

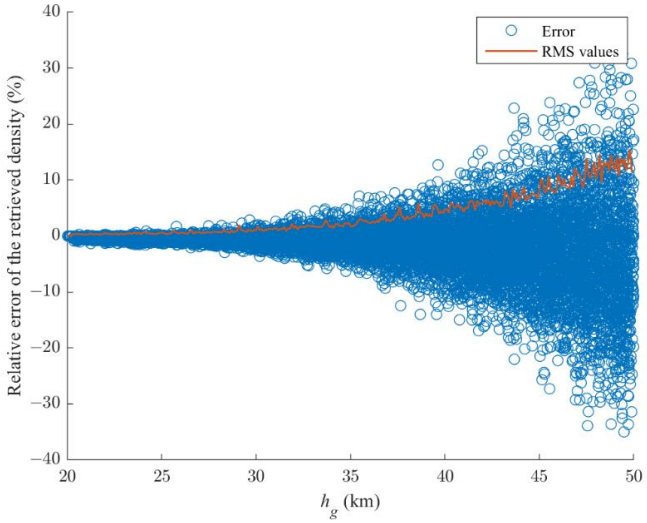

Figure 16. Relative error of the retrieved density with the tangent height.

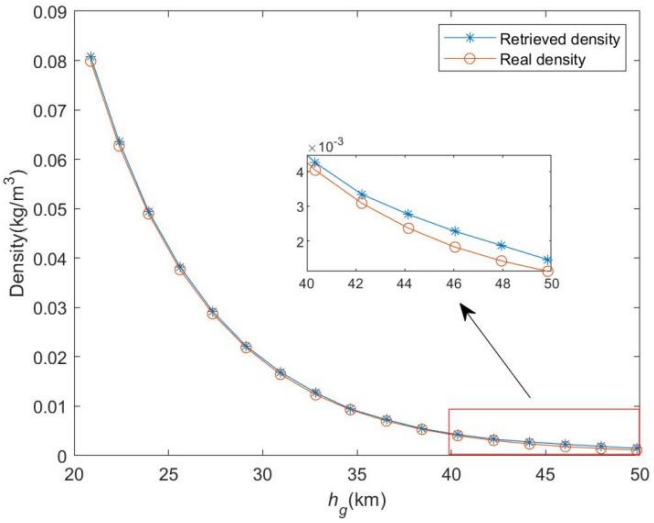

Figure 17. Retrieved density with the tangent height in one simulation.

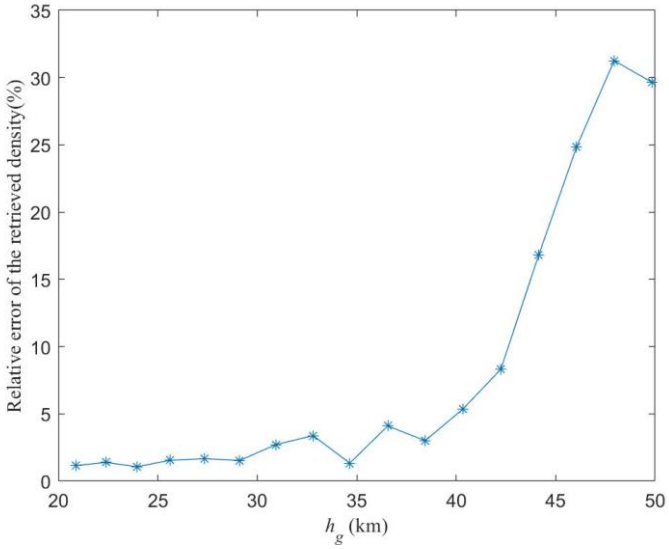

Figure 18. Relative error of the retrieved density with the tangent height in one simulation.

According to the analysis in Section 3, the vertical resolution is 200 m for the retrieval herein. The horizontal coverage percentage in 100 h reaches 96% if the latitudinal and the longitudinal resolutions of the retrieved stratospheric density are 1° and 5°, respectively. In a small region, the spherically stratified atmosphere has little impact on the navigation by the stellar refraction. That is, the impact of the horizontal resolution on the navigation can be neglected if the latitudinal and the longitudinal resolutions of the retrieved stratospheric density are as high as 1° and 5°, respectively. However, the vertical resolution will impact on the navigation directly. Figure 19 depicts the uncertainty on the apparent height with the vertical resolution of the atmospheric data. Herein, as mentioned above, the apparent height acquired by using the atmospheric data with the vertical resolution of 10 m was treated as the reference. That is, the uncertainty on the apparent height with a vertical resolution of the atmospheric data, r_v, is the difference between the apparent height with r_v and that with the vertical resolution of 10 m. In Figure 19, the uncertainty on the apparent height was approximately proportional to the vertical resolution. Hence, both the accuracy of the retrieval and the vertical resolution should be taken into account in evaluating the impact of the retrieved density on the navigation comprehensively. For example, according to simulations, the RMS value of the uncertainty on the apparent height was 166 m if the relative error of the retrieval was 0.9% at the tangent height of 30 km and the vertical resolution was 200 m by the star occultation. However, the RMS value of the uncertainty on the apparent height is 735 m if the relative error of the retrieval is 0.3% under the tangent height of 30 km and the vertical resolution is 1.4 km by the GPS radio occultation. Hence, the retrieval by the star occultation is more suitable for the navigation by the stellar refraction to achieve a higher accuracy than that by the GPS radio occultation.

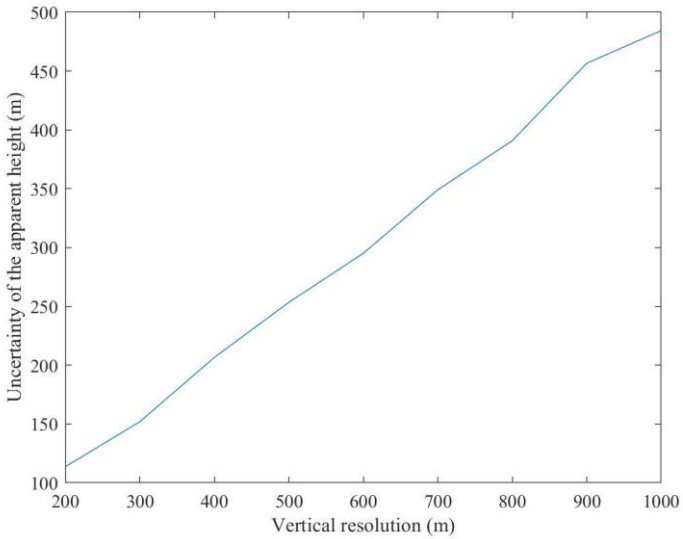

Figure 19. Uncertainty of apparent height with the vertical resolution.

7. Conclusions

Aiming at the navigation by the stellar refraction with the high accuracy, this paper investigates the retrieval of the stratospheric density by the star occultation. After the retrieval was derived in principle, the spatial resolution, the atmospheric attenuation, and the accuracy of the retrieval were analyzed sequentially. The retrieval by the star occultation was proven to be more suitable for the accurate navigation of the stellar refraction than that by the GPS radio occultation by simulations. The following points can be summarized.

(1) The vertical resolution of the retrieval is mainly determined by the orbit and the output frequency of the star sensor. The lower the orbit is and the higher the output frequency of the star sensor is, the higher the vertical resolution is.

(2) The horizontal resolution of the retrieval depends on both the orbit and the star sensor. The longitude interval is determined by the altitude of the satellite. The lower the

orbit is, the smaller the longitude interval is. The coverage of the retrieval in the latitude range is related to the orbital inclination, the right ascension of the ascending node, the direction of the optical axis of the star sensor, and the magnitude threshold of the star sensor. The coverage of the retrieval in the latitude range is large when the optical axis of the star sensor lies in the orbital plane, the polar orbit is employed, and the magnitude threshold of the star sensor is large.

(3) The ray of the starlight in the visible spectrum is attenuated by the refractive dispersion, the molecular scattering, and the ozone absorption mainly when it passes through the stratosphere. The lower the tangent height is, the more significantly the ray of the starlight is attenuated.

(4) The accuracy of the retrieval is mainly impacted by the assumption-derived error, the satellite position error, and the refraction angle error. The satellite position error has little impact on the retrieval error if the accurate GNSS receiver is employed. However, the refraction angle error contributes most of the retrieval error.

In the future, a constellation will be designed for the star occultation. We will also try to verify the retrieval by an on-board experiment if possible.

Author Contributions: Conceptualization, K.W.; methodology, Z.L.; software, S.Z. All authors have read and agreed to the published version of the manuscript.

Funding: This research was funded by National Natural Science Foundation of China, grant number 62173011.

Data Availability Statement: Not applicable.

Conflicts of Interest: The authors declare no conflict of interest.

References

1. Ding, Y.; Chauchat, P.; Pages, G.; Asseman, P. Learning-Enhanced Adaptive Robust GNSS Navigation in Challenging Environments. *IEEE Robot. Autom. Lett.* **2022**, *7*, 9905–9912. [CrossRef]
2. Gounley, R.; White, R.; Gai, E. Autonomous satellite navigation by stellar refraction. *J. Guid. Control Dyn.* **1984**, *7*, 129–134. [CrossRef]
3. White, R.L.; Thurman, S.W.; Barnes, F.A. Autonomous Satellite Navigation Using Observations of Starlight Atmospheric Refraction. *Navigation* **1985**, *32*, 317–333. [CrossRef]
4. Lillestrand, R.L.; Carroll, L.E. Horizon-Based Satellite Navigation Systems. *IEEE Trans. Aerosp. Navig. Electron.* **1963**, *10*, 247–270. [CrossRef]
5. White, R.L.; Tanner, W.E.; Polidan, R.S. Star line-of-sight refraction observations from the Orbiting Astronomical Observatory Copernicus and deduction of stratospheric structure in the tropical region. *J. Geophys. Res. Ocean.* **1983**, *88*, 8535–8542. [CrossRef]
6. Sofieva, V.F.; Kan, V.; Dalaudier, F.; Kyrola, E.; Tamminen, J.; Bertaux, J.L.; Hauchecorne, A.; Fussen, D.; Vanhellemont, F. Influence of scintillation on quality of ozone monitoring by GOMOS. *Atmos. Chem. Phys.* **2009**, *9*, 9197–9207. [CrossRef]
7. Ning, X.; Wang, L.; Bai, X.; Fang, J. Autonomous satellite navigation using starlight refraction angle measurements. *Adv. Space Res.* **2013**, *51*, 1761–1772. [CrossRef]
8. Picone, J.M. Thermospheric densities derived from spacecraft orbits: Accurate processing of two-line element sets. *J. Geophys. Res. Space Phys.* **2005**, *110*. [CrossRef]
9. Jiang, G.Y.; Xu, J.Y.; Shi, D.B.; Wei, F.; Wang, L.Z. Observations of the first meteorological rocket of the Meridian Space Weather Monitoring Project. *Chin. Sci. Bull.* **2011**, *56*, 2131–2137. [CrossRef]
10. Kurihara, J.; Abe, T.; Oyama, K.I. Observations of the lower thermospheric neutral temperature and density in the DELTA campaign. *Earth Planets Space* **2006**, *58*, 1123–1130. [CrossRef]
11. Ramesh, K.; Sridharan, S. Lidar application to middle atmospheric dynamics. *Lidar Remote Sens. Environ. Monit. XV* **2016**, *9879*, 86–96.
12. Liu, T.; Yang, G.; Zhao, Z.; Liu, Y.; Zhou, C.; Jiang, C.; Ni, B.; Hu, Y.; Zhu, P. Design of Multifunctional Mesosphere-Ionosphere Sounding System and Preliminary Results. *Sensors* **2020**, *20*, 2664. [CrossRef]
13. Sokolovskiy, S.V.; Schriener, W.S.; Zeng, Z. Observation, analysis and modeling of deep radio occultation signals: Effects of tropospheric ducts and interfering signals. *Radio Sci.* **2014**, *49*, 954–970. [CrossRef]
14. Collett, I.; Morton, Y.T.J.; Wang, Y.; Breitsch, B. Characterization and mitigation of interference between GNSS radio occultation and reflectometry signals for low-altitude occultations. *Navig. J. Inst. Navig.* **2020**, *67*, 537–546. [CrossRef]
15. Wu, M.J.; Guo, P.; Fu, N.F.; Hu, X.G.; Hong, Z.J. Improvement of the IRI Model Using F-2 Layer Parameters Derived From GPS/COSMIC Radio Occulation Observations. *J. Geophys. Res. Space Phys.* **2018**, *123*, 9815–9835. [CrossRef]

16. Kursinski, E.R.; Hajj, G.A.; Schofield, J.T.; Linfield, R.P.; Hardy, K.R. Observing Earth's atmosphere with radio occultation measurements using the Global Positioning System. *J. Geophys. Res. Atmos.* **1997**, *102*, 23429–23465. [CrossRef]
17. Gorbunov, M.E.; Gurvich, A.S. Microlab-1 experiment: Multipath effects in the lower troposphere. *J. Geophys. Res. Atmos.* **1998**, *103*, 13819–13826. [CrossRef]
18. Jensen, A.S.; Lohmann, M.; Benzon, H.H. Full Spectrum Inversion of radio occulation signals. *Radio Sci.* **2003**, *38*. [CrossRef]
19. Gurvich, A.S.; Brekhovskikh, V.L. Study of the turbulence and inner waves in the stratosphere based on the observations of stellar scintillations from space: A model of scintillation spectra. *Waves Random Media* **2001**, *11*, 163–181. [CrossRef]
20. Salazar, V.; Renard, J.B.; Hauchecorne, A.; Bekki, S.; Berthet, G. A new climatology of aerosols in the middle and upper stratosphere by alternative analysis of GOMOS observations during 2002–2006. *Int. J. Remote Sens.* **2013**, *34*, 4986–5029. [CrossRef]
21. Lair, J.L.; Duchon, P.; Riant, P. Satellite Navigation by Stellar Refraction. *Acta Astronaut.* **1988**, *17*, 1069–1079. [CrossRef]
22. Fischbach, F.F.; Graves, M.E.; Hays, P.B.; Klein, G.S.; Mizgala, C.M.; Peterson, J.W. *Atmospheric Sounding by Satellite Measurements of Stellar Refraction*; Department of Aeronautical and Astronautical Engineering High Altitude Engineering Laboratory, The University of Michigan: Ann Arbor, MI, USA, 1962.
23. Hays, P.B.; Fischbach, F.F. *Analytic Solution for Atmospheric Density from Satellite Measurements of Stellar Refraction*; Department of Aeronautical and Astronautical Engineering High Altitude Engineering Laboratory, The University of Michigan: Ann Arbor, MI, USA, 1963.
24. Fischbach, F.F.; Graves, M.E.; Hays, P.B.; Roble, R.G. *Satellite Measurement of Atmosphereric Structure by Stellar Refraction*; Department of Aeronautical and Astronautical Engineering High Altitude Engineering Laboratory, The University of Michigan: Ann Arbor, MI, USA, 1965.
25. Picone, J.M.; Hedin, A.E.; Drob, D.P.; Aikin, A.C. NRLMSISE-00 empirical model of the atmosphere: Statistical comparison and scientific issues. *J. Geophys. Res. Atmos.* **2002**, *107*, 1468. [CrossRef]
26. Yang, S.; Yang, G.; Zhu, Z.; Jing, L. Stellar Refraction–Based SINS/CNS Integrated Navigation System for Aerospace Vehicles. *J. Aerosp. Eng.* **2016**, *29*, 04015051. [CrossRef]